Experimental evidence of ageing and slow restoration of the weak-contact configuration in tilted 3D granular packings

S. Kiesgen de Richter^{1,†}, V. Yu. Zaitsev², P. Richard¹, R. Delannay¹, G. Le Caër¹ and V. Tournat³

 1 Institut de Physique de Rennes, UMR CNRS 6251, Université de Rennes 1 - 263 av. Général Leclerc, 35042, Rennes, France

 2 Institute of Applied Physics, Russian Academy of Sciences, Uljanova St. 46, 603950, Nizhny Novgorod, Russia

 3 LAUM, CNRS, Université du Maine - av. Olivier Messiaen, 72085, Le Mans Cedex 9, France

[†] Present address: Laboratoire d'Énergétique et de Mécanique Théorique et Appliquée, UMR CNRS 7563, 2 avenue de la forêt de Haye, BP 160, F-54504 Vandœuvre-les-Nancy, France

E-mail: sebastien.kiesgen@ensem.inpl-nancy.fr, vyuzai@hydro.appl.sci-nnov.ru, patrick.richard@univ-rennes1.fr, renaud.delannay@univ-rennes1.fr, vincent.tournat@univ-lemans.fr, gerard.le-caer@univ-rennes1.fr

Abstract. Granular packings slowly driven towards their instability threshold are studied using a digital imaging technique as well as a nonlinear acoustic method. The former method allows us to study grain rearrangements on the surface during the tilting and the latter enables to selectively probe the modifications of the weak-contact fraction in the material bulk. Gradual ageing of both the surface activity and the weakcontact reconfigurations is observed as a result of repeated tilt cycles up to a given angle smaller than the angle of avalanche. For an aged configuration reached after several consecutive tilt cycles, abrupt resumption of the on-surface activity and of the weak-contact rearrangements occurs when the packing is subsequently inclined beyond the previous maximal tilting angle. This behavior is compared with literature results from numerical simulations of inclined 2D packings. It is also found that the aged weak-contact configurations exhibit spontaneous restoration towards the initial state if the packing remains at rest for tens of minutes. When the packing is titled forth and back between zero and near-critical angles, instead of ageing, the weak-contact configuration exhibits "internal weak-contact avalanches" in the vicinity of both the near-critical and zero angles. By contrast, the stronger-contact skeleton remains stable.

PACS numbers: 83.80.Fg, 43.25.+y, 45.70.Ht

Keywords: Granular solids, Nonlinear acoustic probing, Avalanches

1. Introduction

A major issue of industrial and geophysical interest is the knowledge and the understanding of the stability of a granular packing. Evaluating and possibly modifying the stability of a packing is essential to predict for instance avalanches, landslides or the blocking of silos. Even when the external force applied to the packing does not induce a flow, it may drive some microdisplacements as the system adapts to the constraints. These events are precursors of the macroscopic failure; they can change the stress distribution within the packing, thus controlling its stability. The transition from a "static" state to a flowing state is challenging for condensed matter physics. This transition, which can be seen as a "jamming-unjamming transition" with astonishing analogies between granular and glassy systems, has recently triggered a wealth of publications [1, 2, 3, 4, 5, 6].

Granular system driven quasistatically out of equilibrium exhibit memory effects and local, intermittent, rearrangements of grains [7, 8]. Previous works [9, 10, 11] show that parameters like humidity, system dimensions, friction between grains, bottom roughness, or packing fraction can influence the value of the maximum angle of stability of a packing. Aguirre et al. [9] showed that the influence of the number of grain layers on the stability of a packing is noticeable up to about ten layers, while it becomes independent of it for larger layer numbers. The angle at which an avalanche starts was further found to increase with the packing fraction [11]. Scheller et al. [12] observed an evolution of the packing fraction by successive jumps when the tilt angle of a 2D granular monolayer increases. These studies evidence clear signatures of internal reorganizations in a 2D packing and suggest the existence of ageing and memory effects during the inclination process.

Numerical simulations of cyclic tiltings of 2D granular piles emphasized the existence of hysteretic behaviors [7]. They also demonstrated the relevance of the two-phase description, in terms of weak and strong contacts [13], thus correlating with earlier observations [14, 15] which indicate quite independent evolution of the weak- and strong-contact networks. The application of nonlinear acoustic techniques [14] made it possible to detect transitional modifications of the weak-contact fraction in the bulk of granular packings by observing acoustic signal components that had arisen in the material due to its nonlinearity. The key point is that such components are dominated by the weak-contact contribution [16, 17, 18, 15]. The observation of nonlinear acoustic precursors of avalanche approaching agrees well qualitatively with the simulated intermittent modifications of the inter-grain contact network in the bulk of tilted 2D packings [19, 20] and the observations of on-surface displacements [21]. The previous 2D simulation results were reanalyzed in detail by Henkes et al. [22] to examine the link between the avalanche process and a global isostaticity criterion. They emphasized the role of clusters of particles with contacts at the Coulomb threshold, which concentrate the local failure and grow in size when approaching the avalanche. An open question remains as regards whether the contact rearrangements in the bulk

are directly related to the on-surface ones and what the extent of independence of the weak- and strong-contact configurations is.

Here, we demonstrate experimentally the existence of ageing and memory effects at the surface and on the weak contact network. This is done by combining a classical digital imaging techniques [23, 21] as well as a nonlinear acoustic method. In doing so, we prove that experimental results on 3D packings share common features with results of 2D simulations [7, 22].

In section 2 we present the experimental setup and the techniques used to monitor surface activity and modifications of the weak-contact network. Section 3 is devoted to the characterization of the surface of the packing. First, we present the time evolution of the rearranged area due to instantaneous grain motions at the surface of the packing when the latter is inclined from 0° to the angle of avalanche, θ_a . Second, we describe the evolution of the superficial activity during successive tilt cycles between 0 and a given "ageing angle" $\theta_m < \theta_a$. We also depict and discuss the recovery of the activity when the inclination angle exceeds the ageing angle θ_m . Third, we summarize the results obtained and justify the use of non-linear acoustic methods to study the contact network. In section 4 the acoustical measurements are reported. After having compared the information provided by the two methods, we evidence the ageing of the weak-contact network and we describe the occurrence of "mirror-type" rearrangements. Finally, we show that the aged weak-contact configuration exhibits spontaneous restoration towards the initial state when the packing remains at rest for tens of minutes.

2. Experimental Methods

2.1. Experimental set-up

The experimental setup consists of a slowly rotating rectangular plexiglass box containing glass beads (see figure 1). The system is constituted of a heavy table and of a frame which can be inclined at different rates by means of a threaded stem linked to a DC motor. Foams were used to damp vibrations from this motor. The rotation speed can be varied from 0.02° . s⁻¹ to $(1/6)^{\circ}$.s⁻¹. The box, which contains grains, and a camera used to scan the free surface are both fixed on the frame. The inclination angle is measured with an inclinometer fixed also on the frame. The precision of the angle measurement is 0.1°. The size of the box is $30 \times 20 \times 11$ cm. We use glass beads of two types with the same diameter, (3 ± 0.1) mm, similar to those used in experiments [21, 14] as well as smaller beads (2 ± 0.1) mm as in studies [17, 18, 15]. In all experiments, the thickness of the packing is kept constant and equal to 8 cm. The bottom of the box is prepared for once by gluing down glass beads similar to those that constitute the piles on a flat piece of wood. The ambient humidity is kept constant at 50% to avoid effects of capillary or electrostatic forces. To ensure reproducible results, we applied in all experiments the same procedure for the preparation of the packing. First, a grid is put at the bottom of the box, then the box is filled with glass beads and

Experimental evidence of ageing and slow restoration of the weak-contact configuration...4

the height of the packing is made equal to a chosen value. This is done by eroding the free surface with a bar until it reaches the chosen height marked on the lateral walls of the box. Finally, the grid is removed from the box. Glass beads cross the grid and ensure in that way the homogeneization of the packing. Then, the height of the packing is adjusted again as mentioned before. The resulting initial packing fraction (evaluated by measuring the height of the packing) is 0.594 ± 0.001 . During an experiment, the free surface is scanned with a camera interfaced to a computer equipped with an image processing software (ImageJ). The resolution of the camera is 768×512 pixels and 256 gray levels. The acquisition speed can be chosen between 1 and 25 frames s⁻¹. All results based on image-acquisition presented in the present work were obtained with an inclination velocity of 0.05° s⁻¹ and an acquisition rate of 5 frames s⁻¹. These choices are not critical, since we do not observe significant variations of our results when the inclination speed is varied in the aforementioned angular velocity interval.

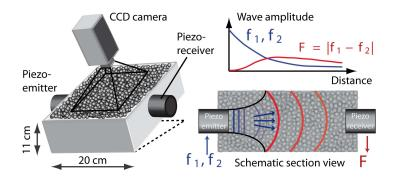


Figure 1. Left: Schematics of the experimental setup. Right: Acoustic probing configuration and spatial dependence of the acoustic frequency components.

2.2. Image processing

The image processing is composed of three steps. First, all images of the movie recorded during the inclination process are extracted. In images, centers of grains appear as bright spots. Each image is subtracted from the next image. In that way, grains which have moved are detected. The elements of the "difference" images correspond to the positions of the centers of grains before and after the rearrangements. Then, these images are binarized and noise is reduced by applying a gray-level thresholding method. To recover the initial size of rearrangements, we apply a dilation algorithm, followed by a hole filling procedure. Finally, a particle analyzer is used to extract the position, the area, and the eccentricity of clusters of synchronously displaced grains. The conversion between pixels and glass bead diameter is obtained by calibration. The above-described image analysis method allows us to evaluate the area fraction which is rearranged between two successive images.

2.3. Acoustical methods

The acoustic method is similar to the one described in [14]. Acoustic pump waves composed of two frequencies f_1 and f_2 are emitted by a piezo-transducer (with an active surface radius a = 1.75 cm) in contact with the beads at mid-depth of the granular layer (see figure 1). A piezo-receiver placed on the opposite wall allows to detect acoustic signals at f_1 , f_2 , as well as some acoustic noise generated in the medium and the difference frequency signal $F = |f_1 - f_2|$ arising from the nonlinearity of the medium [14, 17]. The received signal is recorded using a spectrum analyzer in the form of time dependent spectra, from which the temporal evolutions of specific frequency component amplitudes can be extracted with a 39 ms time step. The emitted frequencies f_1 and f_2 (with an acoustic strain amplitude $\tilde{\varepsilon}_A \simeq 10^{-7}$) are chosen around 10 kHz resulting from a compromise between the efficiency of the transducers and a weak acoustic scattering by the medium. $F = |f_1 - f_2| \simeq 1.5$ kHz is chosen lower than f_1 and f_2 to ensure a low damping in the medium during propagation. Under these experimental conditions, the received acoustic energy is mostly coming from the waves propagating through the grains and their contacts (the solid skeleton) and not through the air. The presence of an in-depth acoustic velocity gradient (due to the nonlinearity of the contacts together with the increasing static pressure with depth [24]), prevents us from giving a simple picture of the acoustic propagation in this configuration. The acoustic propagation is multimodal and the several expected modes are guided by the velocity gradient [24] as well as by the layer boundaries (free boundary at the top, rigid at the bottom). From an estimation of the velocity $v \simeq 100 \text{ m/s}$ of bulk longitudinal waves at a 4 cm depth (static pressure $\simeq 600$ Pa), the wavelength of the emitted waves is $\lambda_{1,2} \simeq 1$ cm. For the nonlinearly generated difference frequency F, the wavelength estimation gives $\Lambda \simeq 8$ cm a value comparable with the layer thickness. We notice that resonance effects between transducers are not observed in gravity stressed granular packings due to the important acoustic damping at these frequencies. The diffraction length of the emitted acoustic beam neglecting the elasticity gradient is $\ell_d = \pi a^2 / \lambda_{1,2} \simeq 10$ cm. Therefore, the difference frequency wave is mainly generated from a collimated pump beam which has not yet reached the free surface of the layer. The nonlinear wave generation is thus expected to be weakly sensitive to the surface events monitored by the camera.

Moreover, as shown in [17, 14] and references therein, there are essential differences in the roles of the weakest contacts and those of the average (and strongly) loaded contacts for the propagation of linear and nonlinear acoustic waves. Let us consider a single Hertzian contact between two beads, with a static deformation ε_0 , and subjected to a dynamic (acoustic) deformation of amplitude $\tilde{\varepsilon}_A$. A Taylor expansion of the Hertz relation [25] for $|\tilde{\varepsilon}_A| \ll |\varepsilon_0|$ provides for the dynamic perturbation, a linear elastic modulus $E^{\ell} \propto \varepsilon_0^{1/2}$ while the nonlinear quadratic modulus is $E^{n\ell} \propto \varepsilon_0^{-1/2}$ [17]. (A typical static pressure of 600 Pa between two of our glass beads gives $\varepsilon_0 \simeq 10^{-6}$ as the average contact strain). Consequently, the smaller the static strain (or stress) of a contact, the higher the contact nonlinearity. Similar reasoning holds for the hysteretic nonlinearity of sheared Hertz-

Mindlin contacts. This explains the numerous experimental observations indicating the dominant role played by the weakest contacts (with $\varepsilon_0 < 10^{-7}$ or less) in the nonlinear acoustic generation process [17, 14, 18, 15]. In particular here, the demodulated F component is selectively sensitive to the weakest contacts in the medium, which in turn makes it sensitive to extremely weak modifications of contact forces induced by tilting. Indeed, although the absolute displacements due to microscopic rearrangements of the grains at the averagely loaded and the weakest contacts are comparable, the relative force change of the averagely loaded contacts induced by tilting is much smaller, which ensures much smaller relative variations of the linear acoustic components.

In summary, the variations of acoustic amplitude of the nonlinearly generated F component discussed in what follows reflect predominantly the variations in the weak contact configuration of the packing. The variations of the acoustic noise amplitude (typically, in the 2 - 3 kHz range and 128 Hz bandwidth, aside of f_1 , f_2 , F and the rotating-engine noise) come from both the surface movements of grains and from structural rearrangements in the bulk. This detected acoustic noise is at least ten times above the measurement noise.

3. Surface measurements

3.1. Dynamics of rearrangements

We describe below experimental results concerning the dynamics of superficial rearrangements during a single inclination of the packing from zero angle until the avalanche onset at θ_a . Figure 2 shows examples of events taking place at the surface of the packing during the inclination from 0° to θ_a . Each subfigure shows all rearrangements which occur between two consecutive images around the inclination angle considered. The number and size of events increase with the inclination angle. While rearrangements are isolated from each other for small inclination angles, those which take place for angles larger than 20° involve a large fraction of the grains located at the surface of the packing. Image analysis techniques, described in the previous section, yield the surface fraction which has evolved between two consecutive images. Figure 3 shows the evolution of the rearranged surface fraction S/S_0 with the angle of inclination of the packing for different experiments performed in similar conditions. Here, S_0 is the total area of the surface of the packing. The rearranged fraction exhibits an overall increase with the inclination angle in a reproducible way. A transition to an intermittent regime, in which large events occur almost periodically, takes place at about 20° . The latter events correspond to the large events named "avalanche precursors" by Nerone et al. [21]. They are due to the simultaneous movement of a large fraction of the grains of the surface of the packing in agreement with the findings of Nerone et al. [21] and of Zaitsev et al. [14]. These authors report indeed that similar large events occur at angles smaller, by a few degrees, than the angle of avalanche. It is worth noticing that similar intermittent events are observed in numerical simulations of inclined 2D packings [20].

Experimental evidence of ageing and slow restoration of the weak-contact configuration...7

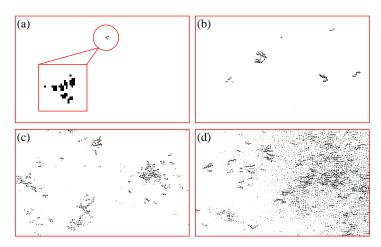


Figure 2. Examples of events observed at the surface of the packing (bead diameter $d = (3 \pm 0.1)$ mm) for different inclination angles. (a) 3° (b) 12° (c) 20° (d) 26° Each subfigure makes visible all rearrangements which occur between two successive images.

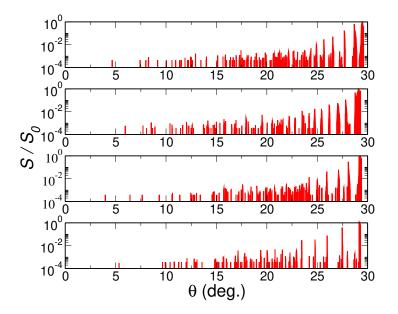


Figure 3. Evolution of the rearranged fraction of the surface with the inclination angle for different experiments carried out in the same conditions (bead diameter $d = (3 \pm 0.1)$ mm).

The results of previous non-linear acoustic studies of Zaitsev et al. [14], those discussed in section 4 and those of 2D numerical simulations of Staron et al. [20] all suggest that these large events are linked to intermittent reorganizations of the network of weak contacts in the bulk of the packing.

To characterize the dynamics and quantify the increase of the rearranged surface fraction during inclination, we show in figure 4, the activity of the packing, $A(\theta)$, defined

Experimental evidence of ageing and slow restoration of the weak-contact configuration...8

as the cumulated sum over the rearranged surface normalized by S_0 .

$$A(\theta) = \sum_{j=0}^{\left\lfloor \frac{\theta}{d\theta} \right\rfloor} \frac{S(jd\theta)}{S_0}.$$
(1)

In equation (1), θ is the angle of inclination of the packing and $d\theta$ is the angular interval between two consecutive images.

Different results found for experiments performed in similar conditions are plotted in figure 4 to emphasize their reproducibility. Three regimes are evidenced in the evolution of the activity of the packing during inclination. First, for small angles, a transient regime depends significantly on the initial preparation of the packing, where some beads initially in metastable positions on the surface move. Second, a growth regime is characterized by an exponential increase of the activity where rearrangements

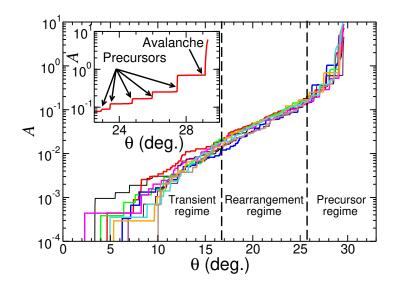


Figure 4. Cumulated sum $A(\theta)$ (bead diameter $d = (3 \pm 0.1)$ mm) for experiments performed in similar conditions. Inset : more detailed record for the last degrees before the avalanche.

involving groups of several beads occur. Third, a regime dominated by the occurence of precursors, with pseudo-periodic large events, appears close to the critical angle. Last, the system avalanches. The most intense precursors occur for angles larger than 25° (figure 4, rightmost dotted line), but the first, less intense, ones are more difficult to detect. The minimum value of the angle at which they can be detected, is of the order of 20° and varies from experiment to experiment (see inset of figure 4). For simplicity, the precursor dominated regime will be named hereafter "precursor regime".

3.2. Evidence of ageing

To study the influence of the system history on the activity of the packing, we applied a series of consecutive forth-and-back tilting cycles to the container. During a cycle, the box is first inclined from the zero angle to an angle θ_m chosen to be close to the critical angle and then it is inclined back to the zero angle. The maximum inclination angle θ_m will be named hereafter the "ageing angle". The activity at the surface of the packing is followed during the part of each cycle with forward tilting. During a given inclination,

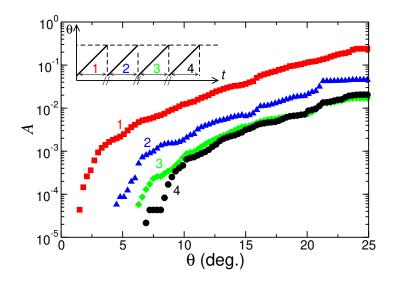


Figure 5. Ageing during several consecutive inclinations of the pile with $\theta_m = 25^{\circ}$ (bead diameter $d = (3 \pm 0.1)$ mm). Each curve is a mean over five independent experiments.

a regular overall increase of the activity of the packing with θ occurs up to θ_m . Figure 5 clearly shows that the system is in a gradually evolving non-stationary state, with an overall activity decrease, during the first three cycles. After four cycles, the activity of the system reaches a limit state corresponding to strongly reduced intensity. The surface is then in a rather stable, "aged" configuration. The system keeps its "aged" configuration when it is inclined between 0 and θ_m . This evolution of the activity of the packing is a clear signature of the existence of the influence of the past history of the system on its future evolution. That phenomenon, which was reported for instance in experiments of granular compaction [26], is typical of evolution of out-of-equilibrium glassy systems. Thus, the activity of a slowly tilted granular packing depends not only on geometrical properties of the packing: bead diameter and box dimensions, initial packing fraction, number of layers, but also on the mechanical perturbations and loading applied to it before it is inclined. Using two-dimensional contact dynamics simulations of packings of discs inclined forth and back during successive cycles, Deboeuf et al. [7] showed that a 2D system driven in that way exhibits an ageing phenomenon related to an anisotropy of the contact orientations. They further show that the latter anisotropy is concentrated in the network of weak contacts. The observed behavior dwells in an asymmetry in the activity of the packing when it is tilted forth and back. The evolution of the contact orientations during the inclination process is irreversible. Contacts tend to orientate in a favored direction which depends on that of gravity. In any case, even if there exists a priori differences between the behavior of 2D and 3D inclined packings, our experiments on inclined 3D packings and numerical simulations of inclined 2D packings

of Deboeuf et al. [7] exhibit similar ageing phenomena. The question of the existence of such an ageing in the weak-contact network will be addressed in section 4.

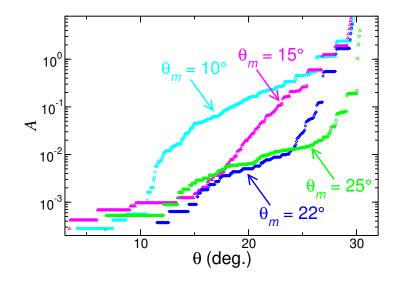


Figure 6. Resurgence of the activity of the packing for various ageing angles $\theta_m = 10^\circ, 15^\circ, 22^\circ, 25^\circ$. The bead diameter is $d = (3 \pm 0.1)$ mm.

To investigate the influence of the ageing angle θ_m on the dynamics of the system, we performed a series of four cycles as described above. The fifth and last cycle differed from the previous ones in that the system was inclined up to the avalanche angle. Figure 6 shows the superficial activity of the packing for various values of the ageing angle θ_m during the last passage. The activity resumes precisely at the point where the inclination angle exceeds θ_m for any value of θ_m ranging between 0 and θ_a . The system keeps in its configuration the memory of the value θ_m through irreversible reorganizations during cycles in the interval $[0; \theta_m]$. The previous observations are in good agreement with the results obtained on granular packings in a slowly rotating drum [8]. No precursors are observed in the aged configuration (i.e. for θ lower than θ_m). However precursors reappear for inclination angles larger than θ_m . Figure 6 shows that precursors occur at angles θ lower than 25° for θ_m less than 25°. By contrast precursors are not evidenced for θ lower than 25° when $\theta_m = 25^\circ$ while they would be expected to appear as they do for the other ageing angles. The disappearance of precursors during the ageing process in the interval $[0; \theta_m]$ (figure 6) highlights the irreversible nature of precursors.

The path to the avalanche of a given packing depends thus on the value of θ_m and shows a hysteretic behavior. The resurgence of the activity shown by figure 6 emphasizes once again the irreversible nature of the reorganizations in an inclined packing.

3.3. Summary

The aforementioned experimental results constitute evidence of the existence of ageing and memory effects in 3D packings slowly driven to their maximum angle of stability. During inclination cycles, the activity of a granular packing decreases and reaches a Experimental evidence of ageing and slow restoration of the weak-contact configuration...11

stationary state.

These results deal exclusively with observations performed at the surface of the packing. Numerical simulations [19, 20, 22] show that approaching avalanche-type instabilities are linked to the nature of the grain-grain contacts in the bulk of the material. To test how relevant the latter results are for real 3D packings, it is necessary to explore the nature of the contacts within the granular medium. Imaging methods, for instance X-ray tomography [27, 28], are unable to characterize the actual nature of a contact (two spheres can be infinitesimally close without touching each other). Photoelasticity allows to visualize the weak and strong force networks in 2D systems but the application of this method to 3D systems is presently beyond reach. To the best of our knowledge the only technique that is able to probe weak contacts (with the average loading of a few percents of the mean value) within the bulk of a granular medium and with a high temporal resolution is the non-linear acoustic method described in [14]. In the next section we will use the latter method to show that similar effects occur in the bulk of the packing. This will allow us to compare the respective roles played by the weak and strong contact networks in the dynamics and consequently their roles in the unjamming transition.

4. Acoustical measurements

4.1. Pre-avalanche variations of the nonlinear signal component

Figure 7 shows an example of the acoustical record obtained during a tilting of the packing for the last 8° before the critical angle. The noise of the avalanche itself which started at 28° is not shown here. The levels of two received frequency components are presented as a function of the tilt angle: the nonlinear demodulated F component and the component f_1 initially excited in the medium. As discussed earlier, in section 2.3, this record illustrates the higher sensitivity of the nonlinear F component, which is preferentially influenced by the contribution of the weakest contacts in the medium (with a static strain of a few percents of the average contact static strain). Quasi-periodical variations (in the form of abrupt drops) of the nonlinear F component amplitude can be easily identified in figure 7 for the last $\sim 4^{\circ}$ before the avalanche. This qualitative trend has been analyzed in [14]. In what follows, in view of the higher sensitivity of the nonlinear signal F component compared to the linear one, we focus on the nonlinear Fcomponent analysis and in some cases on the acoustic noise as well. The abrupt drops in the amplitude of the nonlinear F component play a role analogous to the intensity bursts of the on-surface rearrangements (compare figures 3 and 7). Like what was done for surface precursors (end of section 3.2), we will name hereafter "precursor region" the angular range in which the most intense, quasi-periodical, acoustical drops occur.

In the general case, the level of the demodulated signal is determined by many factors, among which are the number of the weakest contacts and their loading, the amplitude and attenuation in space of the initially excited f_1 and f_2 components,

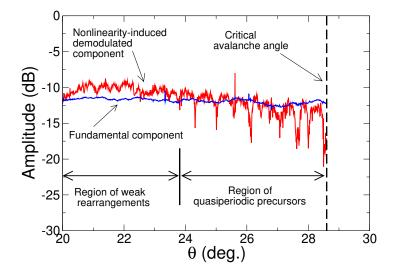


Figure 7. Simultaneously recorded amplitudes of the linear f_1 component initially radiated by the acoustic source and of the F component (nonlinearly demodulated in the material). The latter exhibits stronger variations in the inclined pile for the angular range $20 - 28^{\circ}$. The bead diameter is $d = (3 \pm 0.1)$ mm.

.... Due to the weak amplitude variations of f_1 and f_2 , the dominant contribution to the variation of the F component amplitude is expected to arise from the variations of the nonlinear elastic properties of the packing, i.e. the weak-contact properties. Numerical simulations [19, 20, 22] report the existence of a temporarily unloading, up to complete break, of the "mobilized" weakest contacts during microrearrangements. This observation is consistent with the modeling of the demodulated-signal amplitude of [14] which shows that drops in the nonlinear signal amplitude are produced when the number of weak contacts contributing to the nonlinear acoustic process is temporary diminished. Consequently, abrupt drops in the nonlinear F component amplitude can be interpreted as a temporary decrease in the number of the weakest contacts during the tilt-induced small rearrangements. It should be recalled that to our knowledge, no other experimental technique is able to probe in real time such fast transient variations in the state of the weakest contacts: millisecond time scales (e.g., the time step in figure 7 is 39 ms) and subnanometer scale acoustic displacements.

We now analyze the transition from a noisy-like behavior to a quasi-periodic appearance of drops in the F component amplitude (like in the example shown in figure 7) as a function of the tilt angle. The acoustic signals in different experimental runs exhibit similar trends of variability increase with the tilt angle like in figure 7. Nevertheless the exact positions of the extrema certainly do not coincide (like for the visual records in figure 3). Therefore, it is difficult to directly average such signals in order to extract a general quantitative behavior. In view of this, by analogy with the cumulative characterization of the on-surface activity in the previous section, we characterize statistically the F component amplitude variations with the help of the Hurst parameter [29]. We recall that for a discrete signal Y(u) (with $1 \le u \le N$), the Hurst parameter H(j) within a portion 1 < j < N can be expressed as the ratio between the accumulated peak-to-peak variation R(j) and the standard deviation S(j)[30]:

$$H(j) = R(j)/S(j).$$
(2)

The accumulated peak-to-peak variation R(j) is given by

$$R(j) = \max_{1 \le i \le j} (X_{i,j}) - \min_{1 \le i \le j} (X_{i,j}),$$
(3)

with
$$X_{i,j} = \sum_{u=1}^{u=i \le j} [Y(u) - M_j]$$
, and $M_j = \frac{1}{j} \sum_{u=1}^j Y(u)$. (4)

The standard deviation S(j) is defined by

$$S_j = \left\{ \frac{1}{j} \sum_{i=1}^{j} [Y(i) - M_j]^2 \right\}^{1/2}.$$
(5)

Then the logarithm $\log[H(j)]$ is plotted against $\log(j)$ and the slope of the dependence is determined. This slope is called the Hurst exponent. For a random signal without a trend its value equals to 1/2 (i.e. the normalized peak-to-peak variation increases as a square root of the signal length). If a deterministic trend is present in the signal, the Hurst exponent value becomes close to unity (and such signal is called persistent). A Hurst exponent smaller than 1/2 corresponds to so-called antipersistent signals, for which an increase is likely to be followed by a decrease. The cumulated representation of the Hurst parameter allows to compare different records such as that of figure 7 as well as to distinguish the precursor region from the random noisy-like region.

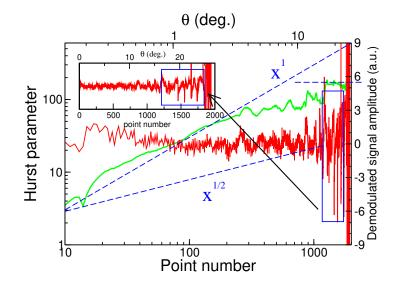


Figure 8. F component acoustic amplitude recorded during tilting up to the critical angle superposed with the corresponding Hurst parameter. The bead diameter is $d = (3 \pm 0.1)$ mm. The inset shows a zoom on a linear scale of the precursor region for which the Hurst parameter stabilizes. The characteristic slopes x^1 , x^0 and $x^{1/2}$ are shown by dashed lines.

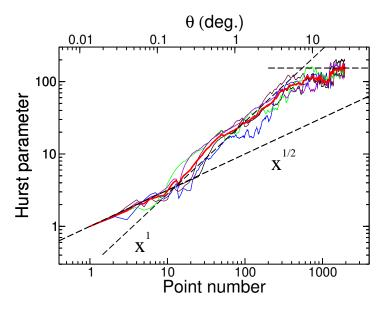


Figure 9. Evolution of the Hurst parameter during the tilting of the packing (bead diameter $d = (3 \pm 0.1)$ mm) from zero to the critical angle. The thick curve shows the average over five records, similar to that in figure 7 but for the same beads. Individual dependences are shown by thin lines. The Hurst parameter stabilizes close to the critical angle. This behavior is observed for the averaged and the individual records. The dashed lines show the characteristic slopes x^1 , $x^{1/2}$, and x^0 .

Figure 8 shows the Hurst parameter for a record similar to the one reported in figure 7. Since the slow signal changes are mostly associated with the slow evolution in the loading of the contacts during the titling, we subtracted the slow trend by averaging over sliding windows of 1/20 of the entire length of the record and then applied the above-described procedure for determining the Hurst parameter. The Hurst parameter stabilizes (a bright antipersistent behavior) in the region of the quasi-periodic drops in the F component amplitude (figure 8). In the initial stage, before the precursors, the signal behavior is closer to a persistent-type behavior with a Hurst exponent close to unity. The thick curve in figure 9 shows the Hurst parameter averaged over five different records (shown by thin lines). The average curve and the individual ones are characterized by a Constant Hurst parameter in the precursor region. Consequently, such a cumulative characteristic appears to be well reproducible over different experimental runs, in contrast to the particular drop features. This constitutes a useful way to determine the onset of precursors and the approaching of the stability loss of the packing.

4.2. Comparative studies of the acoustic signal from the material bulk and of surface rearrangements of the grains

To study the relation between the surface activity and the contact rearrangements in the bulk, simultaneous visual and acoustic measurements were performed both during the ascending and the descending phases. As reported in section 3, in earlier experimental data [21], in nonlinear acoustic observations [14] and in numerical simulations [19, 20] the intensity of the precursors increases when the packing is inclined closer and closer to the angle of avalanche. These

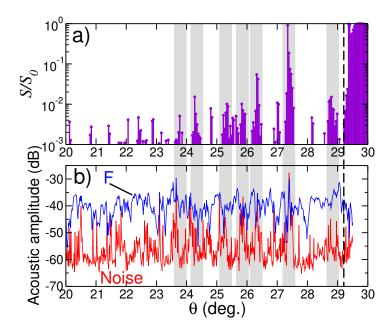


Figure 10. Simultaneously recorded rearranged fraction of the surface S/S_0 (a), and of F variations and acoustic noise around 2816 Hz (b), in the inclined pile for the angular range $20 - 27^{\circ}$ (bead diameter $d = (3 \pm 0.1)$ mm). The gray regions emphasize a high-degree of co-occurrence of variations of the superficial activity, of those of Fdue to weak-contact rearrangements and that of noise bursts.

precursors exhibit a quasi-periodic behaviour and become less frequent than the initial small-amplitude rearrangements. An example of the dependence of the normalized surface activity intensity S/S_0 with the tilt angle of the pile is shown in figure 10(a) while the simultaneously recorded nonlinear F signal and acoustic noise are shown in figure 10(b). The figure shows only the range of large angles $(20^{\circ} - 27^{\circ})$, where the surface activity is significant. For some peaks of the surface activity (marked by gray regions in figure 10), there are simultaneous rapid variations of the F signal related to the weak-contact rearrangements in the material bulk. However, such coincidences are not observed for all peaks, a result which makes the relation of the surface events to the weak-contact rearrangements in the bulk not so obvious. In addition, a significant number of expected correspondences do exist between the on-surface activity and the recorded noise bursts in the tilted pile. We evaluated the correlation function between the peaks in the on-surface activity and the absolute value of the derivative of F with respect to the angle. A rough estimation based solely on three experiments, shows that, for simultaneous records of the two signals, the cross-correlation displays a maximum value of typically 0.25 when the delay time is zero. The correlation-peak amplitude for the visual and acoustic signals recorded for the same tilt appeared to be noticeably greater (≈ 1.5 times) than the amplitude obtained by correlating a visual signal taken

Experimental evidence of ageing and slow restoration of the weak-contact configuration...16

from one tilt and an acoustic signal taken from another, independent tilt. This is an indication that the correlation is weak but discernible. Two facts can explain this weak correlation. First, a large contact reorganisation in the volume (detected by the acoustic method) does not necessary bring out grain motion at the surface (detected by the optical method). Second, large grain displacements at the surface are related to a reorganisation of contacts at the surface which can be more or less correlated to the reorganization of contacts in the volume.

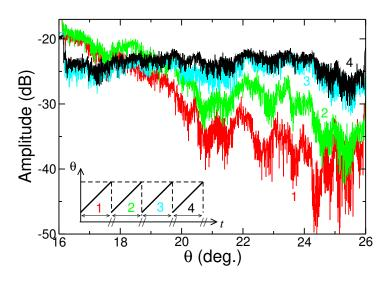


Figure 11. Example of the weak-contact network ageing during several consecutive tilts of the pile as evidenced by the nonlinear F signals shown here for the last 10° before $\theta_m = 26^{\circ}$ (bead diameter $d = (2 \pm 0.1)$ mm).

4.3. ageing of the weak-contact rearrangements in the bulk

As described in section 3, the surface activity exhibits strong ageing after a few consecutive cycles of forth-and-back tilting whith a maximum tilting angle θ_m , smaller than the critical angle of value $\sim 27^{\circ} - 28^{\circ}$. These observations coincide with those of numerical simulations of 2D inclined packings [7, 22]. Deboeuf et al. [7] relate this "ageing" phenomenon to an anisotropy of the contact orientations, concentrated in the network of weak contacts. Even if 2D and 3D systems differ in many respects, it seems reasonable to expect similar behaviors for the bulk rearrangements of the least stable weak-contact subnetworks. Figure 11 shows several such consecutive records of the variability of the weak-contact subnetwork, observed via the nonlinearity produced F signal for $\theta_m = 26^{\circ}$ in the angular range in which F varies the most [14]. The overall amplitude of variation of F is seen to decrease significantly cycle after cycle. Four consequent tilts were sufficient for the weak-contact network to reach an aged configuration, for which no appreciable further variations were noticeable in the angular range studied.

Although four tilts were also found for the ageing of the surface activity (see section 3), it is necessary to wonder whether the transition to the new more stable state

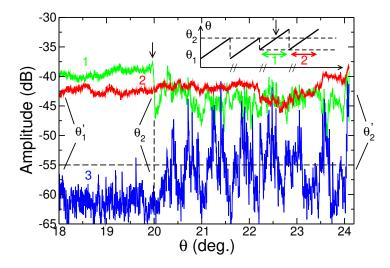


Figure 12. Example of reactivation of the weak-contact network rearrangements upon surpassing the previous upper angle $\theta_2 = 20^\circ$ (curve 1). The noise level (curve 2) is also sensitive to the reactivation. The next upward tilt again exhibits an ageing stage (curve 3). The bead diameter is $d = (2 \pm 0.1)$ mm.

could be caused by the acoustic field itself rather than by the variation in the gravity-field orientation. In order to clarify this, we performed several consecutive tilts of a freshly prepared packing with a several-degree excursion up to a fixed threshold angle below the critical one. After several tilts (for example, in the range $\theta_1 = 14^\circ \le \theta \le \theta_2 = 20^\circ$) the variations in the acoustic signal are strongly reduced like in figure 11. Then the packing is tilted to a larger angle (in the case discussed, the next range is $\theta'_1 = 18^\circ \le \theta \le \theta'_2 = 24^\circ$; see the insert in Figure 12). If the ageing of the weak-contact network resulted from the acoustic perturbation, then the increase in the tilt angle above $\theta_2 = 20^{\circ}$ would not significantly affect the nonlinear acoustic response of the material. Actually, a dramatic change in the material response occurs just upon passing the previous maximal angle of $\theta_2 = 20^\circ$: the intensity of the nonlinear signal variations, which is determined by the intensity of the weak-contact rearrangements, abruptly increases (figure 12). This pronounced effect of the packing orientation indicates the dominant role of gravity in the weak-contact rearrangements. The strong increase in the noise intensity after surpassing the previous maximal tilt angle is also remarkable (see figure 12). Similar behaviors are observed in other overlapped ranges of the tilt angle. As described in section 3, the superficial rearrangements also demonstrate simultaneous reactivation which evidently contributes to the increased noise.

4.4. Formation of a new weak-contact subnetwork and "mirror-type" internal avalanches of the weak-contact network near zero angle

Despite similarities in the responses of the surface and of the bulk to consecutive tiltings, the surface activity and the weak-contact rearrangements differ in some respects. The surface activity decreases strongly during consecutive forth-and-back tiltings of the

The bulk rearrangements of the weak-contact network can behave differently, pile. especially when the pile is tilted in the entire angular range, from zero to a near-crital angle. Figure 13 shows as an example the superimposed records of the F variations during titling from zero to a nearly critical angle of $\theta_m = 26^\circ$ and back from 26° to zero. If the angle is counted from the initial position of the packing (i.e., from $\theta_m = 26^\circ$ for the return to 0°), the two curves exhibit a striking similarity. For the descending phase, a pronounced activity of the weak-contact rearrangements is observed for the angles close to the apparently stable horizontal position of the packing. This observation can be tentatively explained as follows. When coming closer and closer to the nearly critical angle, the configuration of the weak-contact fraction gradually adapts itself to the changing orientation of gravity. In particular, such contacts with "mobilized" dry friction exhibit jumps into new, more stable positions as seen from 2D numerical simulations [19, 20]. For the reorganized weak-contact network, the new stable configuration corresponds to angles close to the critical one. When the angle of the pile decreases back to to zero during the second half-cycle, gravity pushes such contacts out of their stable configuration formed near the critical angle. Therefore, closer to zero angle, such contacts become mobilized. They loose their stability and exhibit a kind of "internal avalanche". They rearrange themselves back to more stable positions corresponding to near-horizontal orientation of the pile. Thus the weak-contact network exhibits very significant modifications. Note that this is not the the case for the network of averagely loaded contacts, which mechanically supports the "visible" structure of the pile and ensures fairly stable conditions for the linear propagation of the sounding signal (i.e., the stable value of the elastic modulus). For a few-degree excursions, ageing of weak-contact rearrangements occurs. By contrast, for sufficiently large excursions of the tilt angles (especially between zero and near-critical angles), the weak-contact network exhibits unceasing rearrangements. We verified that these features are observed for grains of different types whose diameter varies from 1.8 to 3.1 mm (correspondingly the inertia effects differ by over 3.5 times). Such "mirror-type" rearrangements in the bulk, which are seen to show quite good symmetry (figure 13), are fairly reproducible. They do not tend to cease even after 10 - 15 tilt cycles in contrast to the surface activity. However, during the very first tilts of freshly prepared packings, the variations of F normally exhibit finer structure (as shown in the main panel of figure 13). For subsequent mirror-type rearrangements of the weak-contact network, larger scale structures are essentially seen (insets of figure 13).

It is worth noting that if the origin for the return angle is not shifted to zero but counted from the maximum back to zero value, the ascending and descending branches form a kind of antisymmetric hysteretic loop. One can mention a qualitative resemblance to antisymmetric hysteretic loops numerically simulated in [7] (e.g., figure 5 therein) for forth-and-back tilting of 2D granular packings. Note that the quantity reported in [7] (the density of critical contacts) is closely related to the experimentally observed hysteretic behavior, since the variations of the nonlinear acoustic signal are determined by the instability (breaking) of the weak critical contacts.

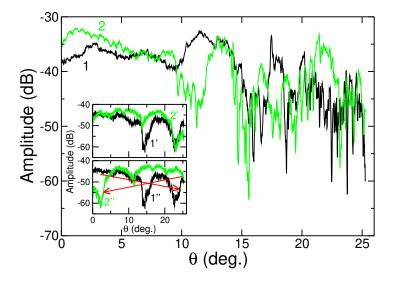


Figure 13. Examples of the symmetrical "mirror-type" evolution of the weak-contact network (bead diameter $d = (3 \pm 0.1)$ mm). The main panel shows superimposed curve 1 for the first tilt from zero to near-critical angle of a freshly prepared packing and the very similar curve 2 for the return. The upper inset shows analogously superimposed curves 1' and 2' for the second up-and-down cycle of tilting in another similar experiment. In the lower inset, for the same pair of the curves, the latter curves have been replotted but the return curve (nammed 2") is now inverted (i.e., the return angle is counted from the maximal value down to zero). The resultant two-branch curve is rather similar to antisymmetric hysteretic loops observed in [7] for other physical characteristics related to the state of the contacts.

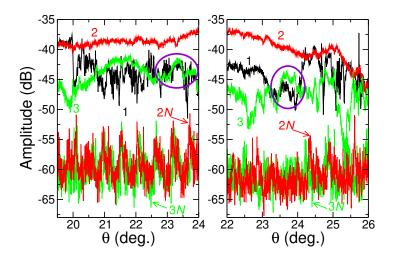


Figure 14. Examples of relaxation of the weak-contact network for two subsequent angular ranges of tilting (bead diameter $d = (2 \pm 0.1)$ mm). Curves 1 are for the first upward tilt in the angular range. Aged curves 2 are recorded after three (left panel) and two (right panel) consecutive up-and-down tilts. Curves 3 are obtained after 20 min (left panel) and 45 min (right panel) of rest at the minimal angle before the next tilt. The noise curves 2N and 3N correspond to curves 2 and 3, respectively.

4.5. Relaxational restoration of aged weak-contact network

Deboeuf et al. [7, 31] observed the relaxation toward a static packing in terms of critical contacts by stopping the rotation. Their 2D numerical simulations show that the density of critical contacts is a dynamical response function to the actual loading. It vanishes after a transient dynamics. The critical contacts likely give rise to microplasticity. In previous experiments [14], the nonlinear acoustic technique revealed active structural rearrangements even in the motionless granular material up to 10 - 30 min after avalanche. It was thus tempting to search for such kinds of relaxation phenomena in our ageing experiment. Despite the essential ageing of the weak-contact network towards an indifferent equilibrium state observed for moderate angular excursions (figures 11 and 13), the weak-contact network tends to spontaneously relax towards the pre-aged structure if the packing remains at rest for sufficiently long time. This statement is illustrated by figure 14. The left part corresponds to a range of tilt angles of $18^{\circ} - 24^{\circ}$, and the right part to the subsequent range of $20^{\circ} - 26^{\circ}$. Curves marked 1 are obtained for the first upward tilt in the angular range indicated. They exhibit pronounced variations due to weak-contact rearrangements (in particular, curve 1 in the left plot in figure 14 is the same as curve 1 in figure 12)

Significantly smoother curves 2 in both parts of figure 14 correspond to aged structures of the weak-contact network obtained after three and two up-and-down cycles for the left and right panels, respectively. Before recording curves marked 3, the packings remained 20 - 45 min at complete rest near their respective minimal angles. Instead of showing changes similar to (or even smaller than) those found for previous cycles, the relaxed curves 3 reveal significantly reactivated rearrangements. Their variations are similar to those of curves 1. In both cases, the weak-contact configurations restore themselves during the rest periods, into states which are close to their states before the first up-tilting. The restored configurations are however not such that curves 3 reproduce entirely the shapes of curves 1. We observe nevertheless similarities between some parts of curves 1 and 3 (e.g. the encircled ones), as well as in the angular positions where abrupt variations occur (intensity jumps). Some features of the aged network appear thus to be restored.

The possibility of such restoration can be understood since the weak-contact rearrangements do not imply macroscopic displacements of the grains, such that almost all contacts remain in positions very close to their initial ones until the onset of the macroscopic avalanche occurs. This ensures the possibility for parts of the weak contacts to return from the aged metastable configuration to the equilibrium positions corresponding to smaller tilt angles. It is important to emphasize that the acoustic signal was switched off during the rest periods. Therefore, the restoration of the aged configuration is attributed to the intrinsic dynamics of the packing under the influence of gravity and thermal fluctuations. The latter factors evidently suffice to overcome energy barriers resulting from the nanometer scale distances between the ruptured and slightly separated interfaces at the weak contacts. Figure 14 shows that this configuration can be spontaneously restored to a considerable extent, even after significant disturbance, if the packing is returned to the initial angle and if it is maintained at rest for a sufficiently long time.

It is also interesting to compare the levels of its own acoustic noise in the tilted packing for the aged and then restored configurations. The own material noise within a 128 Hz bandwidth around 2816 Hz (as in figure 12) is shown in figure 14 by curves marked 2N and 3N which correspond to curves 2 and 3. The noise becomes 3 - 6 dB more intense after the rest period. Comparison with the much stronger noise in freshly prepared packings (figure 12) indicates that the noise is initially dominated by the superficial activity.

5. Conclusions

Optical measurements and non-linear acoustic technique were combined to study destabilization in tilted granular packings. The resulting grain rearrangements at the surface of the pile as well as the modifications of the weak-contact network can be followed in that way. These two signals exhibit weak, although discernible correlations at least for freshly prepared granular piles. These correlations seem to disappear when the piles are inclined repeatedly forth and back. Additional more detailed statistical studies of the on-surface displacements, of the weak-contact network modifications and of the own acoustic noise in granular piles are planned. The reported experiments constitute evidence of the existence of ageing and memory effects in 3D packings slowly driven to their maximum angle of stability. During inclination cycles, the activity of a granular packing decreases (after 3-5 cycles) and reaches a stationary state. For cycles performed in overlapped ranges of the tilt angles, the aged configuration presents reactivation of the rearrangement activity upon surpassing the previous maximal tilt angle. This is observed for the weak-contact network modification as well as for surface activity. For larger excursions, especially for inclinations in the entire range from zero to near-critical angles, very peculiar rearrangements occur in the weak-contact fraction instead of ageing towards an indifferent configuration. These rearrangements appear as "mirror-type internal avalanches" when the packing is tilted up to an almost critical angle and then returned to the horizontal position. For the descending half-cycles, the configuration of weak contacts rearranged during upward tilting loses its stability closer to zero angle producing a kind of "mirror" symmetry of the weak-contact avalanches. This effect does not exhibit any trend toward ceasing and is very well reproducible for multiple forth-and-back cycles, unlike irreversibly aged on-surface displacements. Finally, it is found that even apparently aged configurations of the weak-contact network can exhibit a peculiar slow restoration towards the configuration it had before ageing if the packing remains at rest during tens of minutes. These results have a deep relation to earlier reported relaxation effects of other types found for granular materials [7, 32]. In a broad sense, the experimental results presented support and complement the conclusion following from numerical simulations in 2D [13, 7, 19, 20] and from earlier acoustical

[16, 17] results that granular materials can be viewed as a composition of essentially independent fractions of strong and weak contacts with radically different properties.

Our results suggest that the non-stationary dynamics of an inclined grain packing shares relaxation properties and memory effects with granular media subjected to different kinds of mechanical perturbations (for instance, tapping [26, 33, 34]). ageing effects stabilize the packing. They emphasize the major role played by the orientation of gravity in the reorganization of contact networks. In particular, the activity of the packing was shown to depend strongly on the past of the system. This ageing effect has to be considered in parallel with the influence of the initial preparation of the packing (for example the initial packing fraction). Thus, information on that past is in some way stored in a specific texture of contact between grains.

6. Acknowledgments

The study was supported in parts by ANR grants STABINGRAM, ANR-05-BLAN-0273, NT-05-3-41489, and RFBR-PICS grant No 09-02-91071-CNRS. V.Z. acknowledges the Universities of Maine and Rennes 1 for obtaining invited-professor grants. We thank A. Faisant and E. Brasseur for technical help, D. Bideau, Ph. Boltenhagen and D. Iudin for helpful discussions.

- J. B. Knight, C. G. Fandrich, C.N. Lau, H. M. Jaeger, and S. R. Nagel. Density relaxation in a vibrated granular material. *Phys. Rev. E*, 51(5):3957–3963, May 1995.
- [2] C. S. O'Hern, S. A. Langer, A. J. Liu, and S. R. Nagel. Force distributions near jamming and glass transitions. *Phys. Rev. Lett.*, 86(1):111–114, Jan 2001.
- [3] R. R. Hartley and R. P. Berhinger. Logarithmic rate dependence of force networks in sheared granular materials. *Nature*, 421:928–931, 2003.
- [4] G. Marty and O. Dauchot. Subdiffusion and cage effect in a sheared granular material. Phys. Rev. Lett., 94(1):015701, Jan 2005.
- [5] E.I. Corwin, H.M. Jaeger, and S. Nagel. Structural signature of jamming in granular media. *nature*, 435:1075–1078, 2005.
- [6] N. Xu, V. Vitelli, M. Wyart, A. J. Liu, and S. R. Nagel. Energy transport in jammed sphere packings. *Phys. Rev. Lett.*, 102(3):038001, Jan 2009.
- [7] S. Deboeuf, O. Dauchot, L. Staron, A. Mangeney, and J.-P. Vilotte. Memory of the unjamming transition during cyclic tiltings of a granular pile. *Phys. Rev. E*, 72(5):051305, Nov 2005.
- [8] A. Kabla, G. Debrégeas, J.-M. di Meglio, and T. J. Senden. X-ray observation of micro-failures in granular piles approaching an avalanche. *EPL (Europhysics Letters)*, 71(6):932–937, 2005.
- [9] M. A. Aguirre, N. Nerone, A. Calvo, I. Ippolito, and D. Bideau. Influence of the number of layers on the equilibrium of a granular packing. *Phys. Rev. E*, 62(1):738–743, Jul 2000.
- [10] Ph. Boltenhagen. Boundary effects on the maximal angle of stability of a granular packing. The European Physical Journal B - Condensed Matter and Complex Systems, 12:75–78, 1999.
- [11] M. A. Aguirre, N. Nerone, I. Ippolito, A. Calvo, and D. Bideau. Granular packing: influence of different parameters on its stability. *Granular Matter*, 3(1):75–77, 2001.
- [12] T. Scheller, C. Huss, G. Lumay, N. Vandewalle, and S. Dorbolo. Precursors to avalanches in a granular monolayer. *Phys. Rev. E*, 74(3):031311, Sep 2006.
- [13] F. Radjai, D. E. Wolf, M. Jean, and J.-J. Moreau. Bimodal character of stress transmission in granular packings. *Phys. Rev. Lett.*, 80(1):61–64, Jan 1998.

- [14] V. Yu. Zaitsev, P. Richard, R. Delannay, V. Tournat, and V. E. Gusev. Pre-avalanche structural rearrangements in the bulk of granular medium: Experimental evidence. *EPL (Europhysics Letters)*, 83(6):64003, 2008.
- [15] V. Yu. Zaitsev, V. E. Nazarov, V. Tournat, V. E. Gusev, and B. Castagnède. Luxemburg-gorky effect in a granular medium: Probing perturbations of the material state via cross-modulation of elastic waves. *EPL (Europhysics Letters)*, 70(5):607, 2005.
- [16] V.Yu. Zaitsev. Nonideally packed granular media: Numerical modeling of elastic nonlinear properties. Acoustical Physics, 41(3):385–391, 1995.
- [17] V. Tournat, V. Zaitsev, V. Gusev, V. Nazarov, P. Béquin, and B. Castagnède. Probing weak forces in granular media through nonlinear dynamic dilatancy: Clapping contacts and polarization anisotropy. *Phys. Rev. Lett.*, 92(8):085502, Feb 2004.
- [18] V. Tournat, V. E. Gusev, V. Yu. Zaitsev, and B. Castagnède. Acoustic second-harmonic generation with shear to longitudinal mode conversion in granular media. *EPL (Europhysics Letters)*, 66(6):798, 2004.
- [19] L. Staron, J.-P. Vilotte, and F. Radjai. Preavalanche instabilities in a granular pile. Phys. Rev. Lett., 89(20):204302, Oct 2002.
- [20] L. Staron, F. Radjai, and J.-P. Vilotte. Granular micro-structure and avalanche precursors. Journal of Statistical Mechanics: Theory and Experiment, page P07014, 2006.
- [21] N. Nerone, M. A. Aguirre, A. Calvo, D. Bideau, and I. Ippolito. Instabilities in slowly driven granular packing. *Phys. Rev. E*, 67(1):011302, Jan 2003.
- [22] S. Henkes, C. Brito, O. Dauchot, and W. van Saarloos. Local coulomb versus global failure criterion for granular packings. Soft Matter, 6:2939 – 2943, 2010.
- [23] M. Bretz, J. B. Cunningham, P. L. Kurczynski, and F. Nori. Imaging of avalanches in granular materials. *Phys. Rev. Lett.*, 69(16):2431–2434, Oct 1992.
- [24] V. E. Gusev, V. Aleshin, and V. Tournat. Acoustic waves in an elastic channel near the free surface of granular media. *Phys. Rev. Lett.*, 96(21):214301, Jun 2006.
- [25] K. L. Johnson. Contact Mechanics. Press syndicate of the University of Cambridge, 1987.
- [26] C. Josserand, A. V. Tkachenko, D. M. Mueth, and H. M. Jaeger. Memory effects in granular materials. *Phys. Rev. Lett.*, 85(17):3632–3635, Oct 2000.
- [27] P. Richard, P. Philippe, F. Barbe, S. Bourlès, X. Thibault, and D. Bideau. Analysis by x-ray microtomography of a granular packing undergoing compaction. *Phys. Rev. E*, 68(2):020301, Aug 2003.
- [28] T. Aste, M. Saadatfar, and T. J. Senden. Geometrical structure of disordered sphere packings. *Phys. Rev. E*, 71(6):061302, Jun 2005.
- [29] H.E. Hurst. Long-term storage capacity of reservoirs. Trans. Am. Soc. Civil Eng., 116:770799, 1951.
- [30] P. Embrecht and M. Maejima. Selfsimilar processes. Princeton University Press, Princeton, New-Jersey USA, 2002.
- [31] S. Deboeuf, E.M. Bertin, E. Lajeunesse, and O. Dauchot. Jamming transition of a granular pile below the angle of repose. *The European Physical Journal B - Condensed Matter and Complex* Systems, 36(1):105–113, november 2003.
- [32] L. Bocquet, E. Charlaix, S. Ciliberto, and J. Crassous. Moisture-induced ageing in granular media and the kinetics of capillary condensation. *Nature*, 396(6713):735–737, 1998.
- [33] Ph. Ribière, P. Richard, P. Philippe, D. Bideau, and R. Delannay. On the existence of stationary states during granular compaction. *Eur. Phys. J. E*, 22(3):249–253, mar 2007.
- [34] Ph. Ribière, P. Richard, R. Delannay, D. Bideau, M. Toiya, and W. Losert. Effect of rare events on out-of-equilibrium relaxation. *Phys. Rev. Lett.*, 95(26):268001, Dec 2005.